RSC Advances

ROYAL SOCIETY OF CHEMISTRY

www.rsc.org/advances

ARTICLE

Fabrication of La_2NiO_4 Nanoparticles as an Efficient Bifunctional Cathode Catalyst for Rechargeable Lithium-Oxygen Batteries

Received 00th January 20xx,
Accepted 00th January 20xx

DOI: 10.1039/x0xx00000x

www.rsc.org/

Zhongshan Wei,[a] Yanhui Cui,[a] Kevin Huang,[b] Jue Ouyang,[a] Junwei Wu,*[a] Andrew P. Baker,[a] and Xinhe Zhang[c]

Efficient catalysts for oxygen evolution reaction (OER) and oxygen reduction reaction (ORR) are crucial enabling materials for rechargeable Li-O_2 batteries. In the present work, La_2NiO_4 (LNO) synthesized by hydrothermal process and modified Pechini method were studied as a catalyst for rechargeable Li-O_2 batteries. The catalyst prepared by the hydrothermal method shows smaller particle size and a macroporous structure with 10x higher surface area than that synthesized by the Pechini counterpart, leading to a better electrocatalytic activity. The improved OER catalytic activity of the hydrothermal-LNO nanoparticles was confirmed by a 150 mV lower recharge potential than the Pechini-LNO particles and catalyst-free pure super P (SP) electrode. In addition, the hydrothermal-LNO catalyzed battery cell delivered a first discharge capacity of 14310.9 mAh g^{-1} at 0.16 mA cm^{-2}, compared to 8132.4 mAh g^{-1} of the Pechini-LNO and 7478.8 mAh g^{-1} of pure SP electrode, demonstrating higher catalytic ORR activity of the hydrothermal-LNO particles. Overall, the LNO nanoparticles are promising cathode catalyst for non-aqueous electrolyte based Li-O_2 batteries.

Introduction

Recently, rechargeable lithium-oxygen (Li-O_2) batteries have garnered much attention due to its much higher theoretical energy density than conventional lithium-ion batteries,[1-5] showing promising future applications in all electric vehicles and large-scale energy storage systems.[6-8] However, today's development of Li-O_2 batteries is still at the infant stage. A large number of scientific and engineering challenges in efficiency and durability have not been met.[9-11] One of the fundamental issues causing the inferior performance is the sluggish kinetics of cathode reactions where the ORR and OER take place.[11,12] Seeking a highly efficient ORR and OER catalyst is a key to further advance the Li-O_2 battery technology. By far, significant research effort has been devoted to improving the stability of electrolyte, preventing the oxidation of metal lithium, and developing new cathode catalysts,[10] among which finding a suitable ORR- and OER-active electrocatalyst is perceived vitally important.[13-15] To date, studies on cathode catalysts for non-aqueous electrolyte based rechargeable Li-O_2 batteries have mainly focused on noble metals and their alloys,[16,17] carbon matrix and graphene,[10,18-20] metal oxides and their composites.[21-23]

Perovskite structured oxides (ABO_3) have been historically employed as an effective electrode catalyst for high-temperature solid oxide fuel cells; they have also been investigated as a cathode catalyst for Li-O_2 batteries recently. For example, Zhang and coworkers demonstrated a low charge potential of 3.4 V using porous perovskite $LaNiO_3$ nanocubes as a cathode catalyst.[12] Mai et al. demonstrated that the hierarchical mesoporous perovskite $La_{0.5}Sr_{0.5}CoO_{2.91}$ nanowires were highly efficient catalyst for the ORR with low peak-up potential and high limiting diffusion current,

[a] Department of Materials Science and Engineering, Harbin Institute of Technology Shenzhen Graduate School, Shenzhen Key Laboratory of Advanced Materials, Shenzhen 518055, China. PR China. E-mail: junwei.wu@hitsz.edu.cn
[b] Department of Mechanical Engineering, University of South Carolina, Columbia, SC 29201, USA.
[c] Dongguan McNair Technology Co., Ltd, Dongguan City, Guangdong 523700, China

†Electronic Supplementary Information (ESI) available: The components images of 2032* coin-type cells (Fig. S1) HRTEM images of Pechini-LNO particles (a) and corresponding to select area electron diffraction (SAED) patterns (b) (Fig. S2) Nitrogen adsorption-desorption isotherms and pore size distribution (inset) of Pechini-LNO particles (Fig.S3) CV curves of pure SP, Pechini-LNO particles + SP and hydrothermal-LNO nanoparticles + SP electrode (a). ORR polarization curves of pure SP, Pechini-LNO particles + SP and hydrothermal-LNO nanoparticles + SP electrode (b-d). OER polarization curves of pure SP, Pechini-LNO particles + SP, hydrothermal-LNO nanoparticles + SP on glassy carbon electrode at 1600-rmp rotation rates (e) (Fig.S4).The initial discharge-charge profile lithium-oxygen battery cells with pure SP, Pechini-LNO particles + SP and hydrothermal-LNO nanoparticles + SP electrodes at current density of 0.16mA cm^{-2} and capacity were limited to 1000mAh g^{-1} (Fig.S5). See DOI: 10.1039/x0xx00000x

the lithium-oxygen battery with such catalyst exhibited a high capacity of 11059 mAh g^{-1}.[24,25] Xu *et. al.* showed a rather stable specific capacity of 9000-11000 mAh g^{-1} for up to five cycles and 1000 mAh g^{-1} capacity for 124 cycles with electrospinning-derived porous perovskite $La_{0.75}Sr_{0.25}MnO_3$ nanotubes cathode catalyst.[4] Han et al. displayed that porous $CaMnO_3$ exhibits a low voltage gap of 0.98 V between discharge and charge.[26] In addition, other perovskite oxides, such as, $LaFeO_3$, $Sr_{0.95}Ce_{0.05}CoO_{3-\delta}$, and $Sr_2CrMoO_{6-\delta}$, have also been investigated as an efficient cathode catalyst for Lithium-oxygen batteries.[27-29] On the other hand, layered perovskite such as A_2BO_4, a structure consisting of alternate layer of an ABO_3 and an AO rock salt,[30,31] has also been studied as an ORR and OER catalyst for Li-O_2 batteries. Jung and coworkers investigated doped La_2NiO_4 as a bifunctional electrocatalyst for ORR and OER in an aqueous alkaline electrolyte.[32] In another work, they demonstrated for the first time that $La_{1.7}Ca_{0.3}Ni_{0.75}Cu_{0.25}O_4$ can promote a faster electrochemical oxidation of Li_2O_2 in Li-O_2 batteries with a non-aqueous aprotic electrolyte.[33]

In the present work, we report synthesis and characterization of the LNO nanoparticles by hydrothermal process and LNO particles through Pechini method, respectively, and compare their electrochemical performance as a bifunctional cathode catalyst with catalyst-free pure super P (SP) cathode in a non-aqueous based Li-O_2 battery. The results clearly indicate that the hydrothermal derived LNO nanoparticles are promising cathode catalyst for Li-O_2 batteries.

Experimental

Materials synthesis

Hydrothermal method was used to synthesize LNO nanoparticles. In a typical process, 3.464 g $La(NO_3)_3 \cdot 6H_2O$, 1.412g $Ni(NO_3)_2 \cdot 6\ H_2O$, 1.800 g polyvinyl pyrrolidone (PVP) and 0.900 g glycine were dissolved in 70 ml deionized (DI) water, followed by adjusting the pH value of the solution to 9.9 with $NH_3 \cdot H_2O$. Then the prepared solution was transferred into a 90 ml Teflon-lined autoclave and held for 24 h at 200 ℃. The obtained precipitates were then rinsed alternately with ethanol and DI water for several times and dried at 80 ℃. Finally, the particles were fired at 450 ℃ for 2 h to remove residue organics and at 950 ℃ for another 2 h to form the phase.

The LNO particles were synthesized by a modified Pechini method.[34] In general, the stoichiometric amounts of lanthanum-nitrate and nickel-nitrate were dissolved in a mixture of DI water and ethylene glycol, followed by adding citric acid into the solution with agitation; the molar ratio of critic acid to cation was maintained at 3:1. This solution was stirred continuously at 80 ℃ in a water-bath until a gel was formed. The gel was then dried under vacuum at 200 ℃ for 6 h. After drying, the foam-like residue was collected and pre-fired at 750 ℃ for 4 h to remove organic residues. Finally, LNO catalyst particles were obtained by firing at 1150 ℃ for 4 h.

Structural and morphological characterization

The crystalline structures of the prepared catalysts were examined by X-ray diffraction (XRD) between 2θ=10° and 80° using a Rigaku D/max 2500PC system with Cu radiation (λ=0.15418 nm). Field emission scanning electron microscope (FE-SEM, Hitachi S4700, 15KV) and transmission electron microscope (TEM, JEOL JEM-2100F) were employed to capture morphology. The BET surface area was analyzed by N_2 adsorption-desorption on a surface analyzer (NOVA 2000e).

Electrochemical measurements

Rotating-disk electrode (RDE) measurements were carried out to assess their ORR and OER catalytic activity in aqueous electrolyte. 5 mg of Super P (SP), or 2.25 mg of Pechini-LNO particles mixed with 2.75 mg of SP, or 2.25 mg hydrothermal-LNO nanoparticles with 2.75 mg SP were dispersed in 1 mL of ethonal solvent with 122 μL of 5 wt% Nafion solutions, respectively. Then they were sonicated for at least 30 min to form a homogeneous ink. Cyclic voltammetry (CV) and linear sweep voltammetry were conducted in a three electrode electrochemical cell. Twenty micrograms of sample was loaded on the glassy carbon working electrode (4 mm in diameter), O_2-saturated 0.1 M KOH was used as the electrolyte. Electrochemical data were collected with a CHI 760D electrochemical work station (Shanghai CHI Instrument Company, PR China). The three-electrode cell used for RDE measurements

consists of a platinum electrode as a counter electrode, an Ag/AgCl electrode as a reference electrode.

The LNO-containing oxygen electrodes were prepared by mixing the catalyst LNO particles with a commercial SP and Polyvinylidene Fluoride (PVDF) in a weight ratio of 45:40:15, while N-methyl-2-pyrroli-dinone (NMP) was used as the solvent. For comparison, pure SP was also prepared as a catalyst-free electrode by mixing it with PVDF in a weight ratio of 85:15. The resulting electrode slurry were then uniformly coated on a carbon paper (Gas diffusion layer) and dried in a vacuum oven at 120 ℃ for 4 h to remove residual solvent. The geometric area of the electrode was about 1.53 cm^2 and carbon mass loading in the electrode slurry was controlled within 1.0±0.2 mg cm^{-2}. The specific capacity was calculated based on the total mass of carbon on the electrode. Electrochemical properties of the prepared electrode were evaluated using 2032® coin-type cells assembled in glove box under an Argon atmosphere (<1 ppm H_2O). The cell was consisted of a lithium chip (geometric area about 1.91 cm^2) as the anode, a glass fiber (geometric area about 2.54 cm^2, 2.7 µm pore size) as the separator and a prepared oxygen cathode (see Fig. S1 for the cell assembled). 1 M lithium bis(trifluoromethane sulfonimide) dissolved in tetra(ethylene glycol) dimethyl ether(TEGDME) (or 1 M LiTFSI/TEGDME) was used as the electrolyte. The cells were galvanostatically discharged and charged within a 2.0-4.6 V voltage window with the cathode exposed to a pure oxygen atmosphere.

Results and discussion

Physical characterization

The SEM and TEM images of LNO are displayed in Fig. 1. The LNO nanoparticles derived from hydrothermal approach exhibit macroporous structure with a particle size of 100-200 nm (Fig. 1a, b, e). In contrast, LNO particles derived from modified Pechini method (Fig. 1c, d) shows sub-micron particle size of around 500 nm and non-pore structure. From the HRTEM images of Fig. 1f, it is evident that hydrothermal-LNO nanoparticles show a 0.3808 nm fringe between two adjacent lattices; this is consistent with the (101) plane of LNO. The corresponding SAED analysis shown in Fig. 1g indicates a single-crystallized nature of the as-obtained hydrothermal-LNO. The characteristic diffraction patterns can be assigned to (101), (103) and (110) facets of LNO. The HRTEM images of the modified Pechini method derived LNO particles shown in Fig. S2, indicate the characteristic diffraction rings of corresponding polycrystalline LNO.

The XRD patterns (Fig. 2a) of both hydrothermal-LNO nanoparticles and Pechini-LNO particles particles match well with the standard pattern (PDF# 11-0557) of the layered perovskite-type LNO shown in Fig. 2b without any impurities phase such as La_2O_3 or NiO; this observation is consistent with the SAED results.

The surface area of a catalyst plays an important role in the catalytic activity and discharge capacity of Li-O_2 batteries.[35,36] As shown in Fig. 2c, the BET surface area of hydrothermal-LNO nanoparticles is 10.01 m^2 g^{-1}, nearly 10 times the Pechini-LNO particles (0.977 m^2 g^{-1}) (see Fig. S3). The two insets of Fig. 2c and Fig. S3 are the corresponding pore size distributions. The pore volume of the hydrothermal-LNO is (0.027 cc/g) 10 times higher than that of pechini-LNO (0.002 cc/g). For the N_2 adsorption desorption isotherms, both of the catalysts present typical-V N_2 sorption isotherms with distinct H3 hysteresis loops that can be linked to the pores between the LNO particles formed when these particles stacked lap together. Additionally, the pore size distribution calculated using the BJH method show that hydrothermal-LNO was composed of porous composites with a narrow distribution centered at approximately 180nm, and pechini-LNO centered at approximately 180nm and 40-80 nm. For comparison, the surface area of SP carbon, 67.5 m^2 g^{-1}, is much higher than both types of LNO catalysts.

Electrochemical performances

To assess the ORR and OER catalytic activity, we used RDE measurements in aqueous electrolyte system with O_2-saturated 0.1 M KOH. Fig. S4a shows the CV curves of three electrodes (pure SP, Pechini-LNO particles + SP, hydrothermal-LNO nanoparticles + SP) at a scan rate of 10 mV s^{-1} in the range of -1.0 ~ 0.2 V Vs. Ag/AgCl electrode (r = 0 rpm). The curve of hydrothermal-LNO nanoparticles + SP electrode exhibit more positive ORR peak potential than pure

SP and Pechini-LNO particles + SP electrodes, as shown in Fig. S4a. Fig. S4b-d shows the linear sweep voltammograms of three electrodes as RDE obtained under various rotating rate from 400 to 1600 rpm, respectively. It is noted that the hydrothermal-LNO nanoparticles show higher response current density compared with the other two electrodes. Furthermore, the OER polarization curves of three electrodes on glassy carbon electrodes were compared in the range of 0.2~2.0 V Vs. Ag/AgCl at r = 1600 rpm, as shown in Fig. S4e. It is obviously that the hydrothermal-LNO nanoparticles + SP electrode has the highest limiting diffusion current. Such results confirmed that the hydrothermal-LNO nanoparticles have better ORR and OER catalytic activities compared with pure SP, Pechini-LNO particles.

The electrochemical performances of Li-O_2 batteries with hydrothermal-LNO nanoparticles and Pechini-LNO particles as the cathode catalyst were measured in a voltage window of 2.0-4.6 V in oxygen atmosphere at room temperature. As a comparison, the performance of a battery with catalyst-free pure SP electrode was also measured under the same condition. Fig. 3a show the first-cycle discharge-charge profiles of the cells operated at a current density of 0.16 mA cm^{-2} with pure SP, Pechini-LNO particles + SP and hydrothermal-LNO nanoparticles + SP cathodes, respectively. The first-cycle discharge specific capacity with hydrothermal-LNO nanoparticles + SP electrode achieved 14310.9 mAh g^{-1}, much higher than 8132.4 mAh $g^{-1}$of the Pechini-LNO particles + SP and 7478.8 mAh g^{-1} of catalyst-free pure SP electrode. Even though discharge-charge cycles of all the batteries were tested in a full voltage window between 2.0 to 4.6 V, the battery with the hydrothermal-LNO catalyst still retained a considerable amount of reversible specific capacity over 2500 mAh g^{-1} after five cycles. In contrast, Fig. 3b shows the battery with catalyst-free pure SP and the Pechini-LNO catalysts with a sharp capacity fading. The enhanced discharge performance of the hydrothermal-LNO nanoparticles + SP cathode was attributed to its high surface areas that provide more favorable catalytic activity sites for a fast reaction. This feature promotes the formation and decomposition of the discharge product Li_2O_2, leading to an increased utilization of carbon materials in the electrode.[37] In addition, during the charge process, Fig. 3a shows a first-cycle specific capacity of 9985.9 mAh g^{-1} with hydrothermal-LNO catalyst, higher than 1153.4 mAh g^{-1} of Pechini-LNO catalyst and 438.5 mAh g^{-1} of catalyst-free pure SP. The first-cycle charge voltage plateau of the hydrothermal-LNO catalyst was about 4.4 V, in comparison to non-plateau for Pechini-LNO catalyst and catalyst-free pure SP electrode below 4.6 V of the upper cut-off voltage. It is also demonstrated that the OER overpotential for hydrothermal-LNO nanoparticles + SP electrode was much lower than Pechini-LNO particles + SP and catalyst-free pure SP electrode. The reduced ORR and OER overpotential suggests that the hydrothermal-LNO is a promising cathode catalyst for Li-O_2 batteries.

The high catalytic activity of LNO can be attributed to high oxygen transport/exchange properties of Ruddlesden-Popper layered perovksite structure.[38] Bruce et al. demonstrated that LiO_2 is an intermediate product during charge/discharge of a nonaqueous Li-O_2 battery. Considering that O_2^- has a high activity and LiO_2 is not stable, Eq. ($O_2 + e^- \rightarrow O_2^-$) is the rate-controlling step.[24] Therefore, to enhance oxygen adsorption or O_2^- formation could definitely improve the ORR catalyst activity. Firstly, lots of oxygen vacancies in the LNO lattice can decrease the repulsion between absorbed O and Lattice O[32], and facilitate interstitial oxygen migration and surface atomic arrangement, thus leading to enhanced oxygen chemisorption. Secondly, the perovskite nanoparticles are beneficial to Li^+ diffusion and the formation rate of LiO_2 and Li_2O_2. Therefore, the catalytic activity was significantly promoted for discharge process.[24,38]

During the charge process, since the oxygen atoms in LNO are loosely bounded in the lattice, the OER may take place with the aid of surface lattice oxygen at low activation energy, therefore LNO promotes the charge process.[32]

In all kinds of lithium batteries, the depth of discharge can significantly affect cycle stability.[37] For Li-O_2 batteries, there is no exception. An over-lithiation can lead to an over-growth of discharge products, such as Li_2O, Li_2O_2, which can impede the transport of Li ions into/out the cathode or blockage of the oxygen diffusion path,[39-41] thus negatively impacting the reversibility of cathode.[11] In order to

study the over-growth of discharge products induced by deep discharge, we carried out galvanostatic discharge-charge cycling experiments with a cut-off capacity of 1000 mAh g^{-1} at a current density of 0.16 mA cm^{-2}, the results are shown in Fig. 4a. The Li-O_2 battery with hydrothermal-LNO catalyst can cycle at least 26 time, whereas, Pechini-LNO catalyst and catalyst-free pure SP suffered a sharp capacity fading starting from the 17th, 13th cycles, respectively. This observation proves again that hydrothermal-LNO nanoparticles is an efficient catalyst for the reversible formation and decomposition of Li_2O_2.

The discharge-charge profiles of Li-O_2 battery with the hydrothermal-LNO catalyst (Fig. 4b) exhibits relatively lower OER discharge-charge potential gap and higher round-trip efficiency than other two (see Fig.S5). It also shows that the hydrothermal-LNO can retain more charge-discharge cycles other two. The discharge-charge gap of the first-cycle was 1.5 V, with a lower charge capacity the corresponding discharge one, implying incomplete decomposition of Li_2O_2 during the charging process. It may be related to tiny amount of Li_2O_2 (in the first discharge) reacted with activated carbon, to produce irreversible Li_2CO_3. Then in the following charge process, less amount of Li_2O_2 decomposed in OER to a smaller capacity.[42-43] Additionally, the charge voltage of the electrode reached the limit voltage of 4.6 V before Li_2O_2 can completely decompose. Therefore, the charge capacity cannot reach the same value as the discharged. After several cycles, the discharge-charge potential gap was reduced as a result of reduced charge potential gap. At the 10^{th} cycle, the discharge-charge potential gap was reduced to 1.0 V, which is slightly higher than some of precious metal catalysts such as Pt/Au nanoparticles and Pt/C.[44,45] However, the stability of electrolyte, passivation of oxygen electrodes and oxidation of lithium foil can also affect the performance of Li-O_2 battery. The discharge voltage decayed noticeably after 25^{th} cycle with the final voltage of discharge dropping from ~2.6 to 2.0 V.

In order to further verify the good ORR catalytic activity of the hydrothermal-LNO, the discharge profiles with the three kinds of electrodes were tested at current densities of 0.08, 0.32, and 0.8 mA cm^{-2} between a voltage window 2.0 and 3.2 V, respectively; the results are shown in Fig. 5. The batteries with the hydrothermal-LNO catalyst exhibit the highest capacity for all the current densities operated, i.e. 14252 mAh g^{-1} at 0.08 mA cm^{-2} shown in Fig. 5a, nearly twice the Pechini-LNO (7327 mAh g^{-1}) and pure SP electrode (5956 mAh g^{-1}). Similar results were also obtained at 0.32 and 0.8 mA cm^{-2} shown in Fig. 5b and 5c, respectively. In addition, in all the profiles of different current densities, we found hydrothermal-LNO nanoparticles + SP electrode possessed the lowest ORR potential gap. In comparing the two synthesized LNO, the enhanced ORR performances of the hydrothermal one can be ascribed to its synergistic effect of smaller particles size, higher surface area, better conductivity and macroporous structure.

The electrochemical mechanism of Li-O_2 batteries typically involves the following redox reactions[46]:

Anode reaction: $Li \leftrightarrow Li^+ + e^-$ [1]

Cathode ORR: $Li^+ + e^- + O_2 \rightarrow LiO_2$ [2]

$Li^+ + e^- + LiO_2 \rightarrow Li_2O_2$ [3]

Cathode OER: $LiO_2 \rightarrow Li^+ + e^- + O_2$ [4]

$Li_2O_2 \rightarrow 2Li^+ + 2e^- + O_2$ [5]

The reactions [2]-[3] and [4]-[5] takes place in the process of ORR and OER, respectively. In order to understand the reaction process, CV curves of the battery with three different electrodes were measured and are shown in Fig. 6. Generally, lithium ion batteries can exhibit CV curves with one cathodic and one anodic peak. It is also common for Li-O_2 batteries to exhibit one cathodic peak and two or three anodic peaks.[47] Here, two broad anodic peaks are observed in Fig.6, consistent with the report by Abaham and co-workers.[48] The CV results of glassy carbon electrode in 0.025 M LiTFSI doped O_2-saturated EMITFSI show two anodic peaks at 3.2 and 3.6 V versus Li^+/Li, which is attributed to reactions [4] and [5], respectively. Therefore, the oxidation peak 1 and peak 2 can be assigned to the reactions [5] and [4], respectively.[49,50]

Taking into account of the fact that Li_2O_2 is the principal discharge products, a different explanation has been proposed to explain the two oxidation peaks from the point of view of the bulk and interfacial Li_2O_2.[51,52] According to this hypothesis, the oxidation peak 1 can be assigned to the interfacial Li_2O_2 located between the bulk Li_2O_2 and carbon or catalyst surface, whereas oxidation peak 2 is considered as the bulk Li_2O_2 oxidation at higher potential.

Nevertheless, from the Fig. 6, one can see that during the charge process Pechini-LNO catalyst can only reduce the potential of anodic peak 2 by about 0.21 V in comparison to catalyst-free of pure super P cathode, whereas the hydrothermal-LNO catalyst displays 0.2 V less potential in anodic peak 1 and about 0.3 V less in anodic peak 2 than the catalyst-free of pure SP electrode. This is consistent with Fig. 3(a) where hydrothermal-LNO catalyst exhibits the lowest charge voltage and the highest charge capacity. Therefore, it is safe to conclude that the hydrothermal-LNO catalyst has the better OER catalytic activity to the decomposition of Li_2O_2 than Pechini-LNO catalyst.

To identify the discharge-charge products of the Li-O_2 batteries with hydrothermal-LNO nanoparticles + SP electrode, XRD patterns of the pristine, the one after the first cycle discharge, and the one after the first cycle charge were displayed in Fig. 7. The charge and discharge are operated under a current density of 0.16 mA cm^{-2}. Comparing with the pristine one, the 1st discharged electrode shows some additional diffractions peaks centered at 23.32°, 32.9°, 35.0°, 40.6°, and 58.68°, which can be indexed to (002), (100), (101), (102), and (110) peaks of Li_2O_2 (PDF#09-0355), respectively. It indicates that Li_2O_2 is the major discharge products. After the 1st charge, the diffraction peaks of Li_2O_2 disappeared completely due to the decomposition of the formed Li_2O_2 during charge process. This further confirms that the discharge-charge process of Li-O_2 batteries involve actually a reversible formation and decomposition of Li_2O_2.

Conclusions

In summary, LNO nanoparticles synthesized via hydrothermal process is a promising bifunctional electrocatalyst for Li-O_2 batteries. Compared with LNO particles prepared by Pechini method and the catalyst-free pure SP electrode, the battery with the hydrothermal-LNO nanoparticles catalyst exhibits much higher capacity, improved round-trip efficiency and longer cycle life. The battery delivers a high discharge capacity of 14310.9 mAh g^{-1} and a charge capacity of 9985.9 mAh g^{-1} at a current density of 0.16 mA cm^{-2}, and the capacity can still be 12731.0 mAh g^{-1} at 0.32 mA cm^{-2}. At a greater current density of 0.8 mA cm^{-2}, the discharge voltage of hydrothermal-LNO + SP electrode was 50 mV higher than that of catalyst-free pure SP. Furthermore, at a cut-off capacity of 1000 mAh g^{-1} operated at 0.16 mA cm^{-2}, hydrothermal-LNO nanoparticles + SP electrode can retain 26 discharge-charge cycles without capacity fading in comparison to 17 and 13 cycles for Pechini-LNO particles + SP and pure SP electrode, respectively. All of the results demonstrate that LNO nanoparticle with good ORR and OER catalytic activity is a promising cathode catalyst for non-aqueous electrolyte based Li-O_2 batteries.

Acknowledgements

This work is supported by the International Collaboration Program of Shenzhen (GJHZ20150312114008636, GJHZ20130411141529167), Shenzhen Peacock Plan Program (KQCX20140521144358003), Fundamental Research Program of Shenzhen (JCYJ20140417172417144, JCYJ20130329141705731), Innovation Institutions Construction Projects of Nanshan District, Shenzhen City (KC2015ZDYF0009A) and the project of Innovative group for high-performance lithium-ion power batteries R&D and industrialization of Guangdong Province (Grant No. 2013N079).

Notes and references

[1] P. G. Bruce, S. A. Freunberger, L. J. Hardwick and J. M. Tarascon, Nature Mater. 2012, **11**, 19.

[2] F. Cheng and J. Chen, Chem. Soc. Rev. 2012, **41**, 2172.

[3] A. Kraytsberg and Y. Ein-Eli, J. Power Sources 2011, **196**, 886-893.

[4] J. J. Xu, D. Xu, Z. L. Wang, H. G. Wang, L. L. Zhang and X. B. Zhang, Angew. Chem. Int. Ed. 2014, **53**, 3887.

[5] M. A. Rahman, X. J. Wang and C. Wen, J. Appl. Electrochem. 2014, **44**, 5-22.

[6] H. G. Jung, J. Hassoun, J. B. Park and Y. K. Sun, B. Scrosati, Nat. 2012, **4**, 579.

[7] H. Cheng and K. Scott, J. Power Sources 2010, **195**, 1370.

[8] S. S. Zhang and D. Foster, J. Power Sources 2010, **195**, 1235.

[9] Y. Shao, S. Park, J. Xiao, J. G. Zhang, Y. Wang and J. Liu, ACS Catal. 2012, **2**, 844.

[10] B. D. McCloskey, D. S. Bethune, R. M. Shelby, T. Mori, R. Scheffler, A. Special, M. Sherwood and A. C. Luntz, J. Phys. Chem. Lett. 2012, **3**, 3043.

[11] J. Jung, K. Song, D. R. Bae, S. W. Lee, G. Lee and Y. M. Kang, Nanoscale 2013, **5**, 11845.

[12] J. Zhang, Y. B. Zhao, X. Zhao and Z. L. Liu, W. Chen, Sci. Rep. 2014, 4, DOI:10.1038/srep05310.

[13] A. Kraytsberg and Y. Ein-Eli, J. Power Sources 2011, **196**, 886.

[14] B. Scrosati, J. Hassoun and Y. K. Sun, Energy Environ. Sci. 2011, **4**, 3287.

[15] F. Cheng and J. Chen, Chem. Soc. Rev. 2012, **41**, 2172.

[16] B. G. Kim, H. J. Kim, S. Back, K. W. Nam, Y. Jung, Y. K. Han and J. K. Choi, Sci. Rep. 2014, 4, DOI:10.1038/srep04225.

[17] Y. Lei, J. Lu, X. Y. Luo, T. P. Wu, P. Du, X. Y. Zhang, Y. Ren, J. G. Wen, D. J. Miller, J. T. Miller, Y. K. Sun, J. W. Elam and K. Amine, Nano Lett. 2013, **13**, 4182.

[18] G. Wu, N. H. Mack, W. Gao, S. Mao, R. Zhong, J. Han, J. K. Baldwin and P. Zelenay, ACS Nano 2012, **6**, 9764.

[19] L. Wang, X. Zhao, Y. H. Lu, M. W. Xu, D. W. Zhang, R. S. Ruoff, K. J. Stevenson and J. B. Goodenough, J. Electron. Soc. 2011, **158**, A1379.

[20] Y. G. Wang, L. Cheng, F. Li, H. M. Xiong and Y. Y. Xia, Chem. Mater. 2007, **19**, 2095.

[21] G. Q. Zhang, J. P. Zheng, R. Liang, C. Zhang, B. Wang, M. Au, M. Hendrickson and E. J. Plichta, J. Electronchem. Soc. 2011, **158**, A822.

[22] A. Débart, J. Bao, G. Armstrong and P. G. Bruce, J. Power Sources 2007, **174**, 1177.

[23] A. Débart, A. J. Paterson, J. Bao and P. G. Bruce, Angew. Chem. Int. Ed. 2008, **120**, 4597.

[24] Y. Zhao, L. Xu, L. Mai, C. Han, Q. An, X. Xu, X. Liu, Q. Zhang, P. Natl. Acad. Sci. USA, 2012, **109**, 19569.

[25] Z.L. Wang, D. Xu, J.J. Xu, X.B. Zhang, Chem. Soc. Rev., 2014, **43**, 7746.

[26] X. Han, Y. Hu, J. Yang, F. Cheng, J. Chen, Chem. Commun., 2014, **50**, 1497.

[27] J.J. Xu, Z.L. Wang, D. Xu, F.Z. Meng, X.B. Zhang, Energy Environ. Sci., 2014, **7**, 2213.

[28] W. Yang, J. Salim, S. Li, C. Sun, L. Chen, J. B. Goodenough, Y. Kim, J. Mater. Chem., 2012, **22**, 18902.

[29] Z. Ma, X. Yuan, L. Li, Z.F. Ma, Chem. Commun. 2014, **50**, 14855.

[30] M. S. D. Read, M. S. Islam, F. King and F. E. Hancock, J. Phys. Chem. B 1999, **103**, 1558.

[31] M. S. D. Read, M. S. Islam, G. W. Watson and F. E. Hancock, J. Mater. Chem. 2001, **11**, 2597.

[32] K. N. Jung, J. H. Jung, W. B. Im, S. Yoon, K. H. Shin and J. W. Lee, ACS Appl. Mater. Interfaces 2013, **5**, 9902.

[33] K. N. Jung, J. I. Lee, W. B. Im, S. Yoon, K. H. Shin and J.W. Lee, Chem. Commun. 2012, **48**, 9406.

[34] M. Pechini, U. S. Patent No. 3,330,697, July 11, 1967.

[35] S. Meini, M. Piana, H. Beyer, J. Schwämmlein and H. A. Gasteiger, J. Electrochem. Soc. 2012, **159**, A302.

[36] Z. Ma, X. Yuan, L. Li and Z.F. Ma, Chem. Commun. 2014, **50**, 14855.

[37] C. O. Laoire, S. Mukerjee, E. J. Plichta, M. A. Hendrickson and K. M. Abraham, J. Electrochem. Soc. 2011, **158**, A302.

[38] X. Ma, B. Wang, E. Xhafa, K. Sun, E. Nikolla, Chem. Commun., 2015, **51**, 137

[39] Y. Liu, L. J. Cao, C. W. Cao, M. Wang, K. L. Leung, S. S. Zeng, T. F. Hung, C. Y. Chung and Z. G. Lu, Chem. Commun. 2014, **50**, 14635.

[40] R. Black, J. H. Lee, B. Adams, C. A. Mims and L. F. Nazar, Angew. Chem. 2013, **125**, 410.

[41] F. J. Li, D. M. Tang, Y. Chen, D. Golberg, H. Kitaura, T. Zhang, A. Yamada and H. S. Zhou, Nano Lett. 2013, **13**, 4702.

[42] Y. Cao, M.S. Zheng, S.R. Cai, X.D. Lin, C. Yang, W.Q. Hu, Q.F. Dong, J. Mater. Chem. A, 2014, **2**, 18736.

[43] M.M. Ottakam Thotiyl, S.A. Freunberger, Z.Q. Peng, P. G. Bruce, J. Am. Chem. Soc., 2012, **135**, 494.

[44] Y. C. Lu, Z. C. Xu, H. A. Gasteiger, S. Chen, K. Hamad-Schifferli, Y. Shao-Horn and J. Am. Chem. Soc. 2010, **132**, 12170.

[45] B. D. McCloskey, R. Scheffler, A. Speidel, D. S. Bethune, R. M. Shelby and A. C. Luntz, J. Am. Chem. Soc. 2011, **133**, 18038.

[46] J. S. Hummelshøj, J. Blomqvist, S. Datta, T. Vegge, J. Rossmisl, K. S. Thygesen, A. C. Luntz, K. W. Jacobsen and J. K. Norskøv, J. Chem. Phys. 2010, **132**, 071101.

[47] S. Ferrari, E. Quartarone, C. Tomasi, M. Bini, P.Galinetto, M. Fagnoni and P. Mustarellii, J. Electronchem. Soc. 2015, **162**, A3001.

[48] C. J. Allen, S. Mukerjee, E. J. Plichta, M. A. Hendrickson and K. M. Abraham, J. Phys. Chem. Lett. 2011, **2**, 2420.

[49] C. Shen, Z.Y. Wen, F. Wang, K. Rui, Y. Lu, X.W. Wu, J. Power sources, 2015, **294**, 593.

[50] D.Y. Zhai, H.-H. Wang, J.B. Yang, K.C. Lau, K.X. Li, K. Amine, L.A. Curtiss, J. Am. Chem. Soc., 2013, **135**, 15364.

[51] F.F. Tu, J. Xie, S.C. Zhang, G.S. Cao, T.J. Zhu, X.B. Zhao, J. Mater. Chem. A, 2015, **3**, 5714.

[52] E. J. Nemanick, J. Power sources 2014, **247**, 26.

Figures

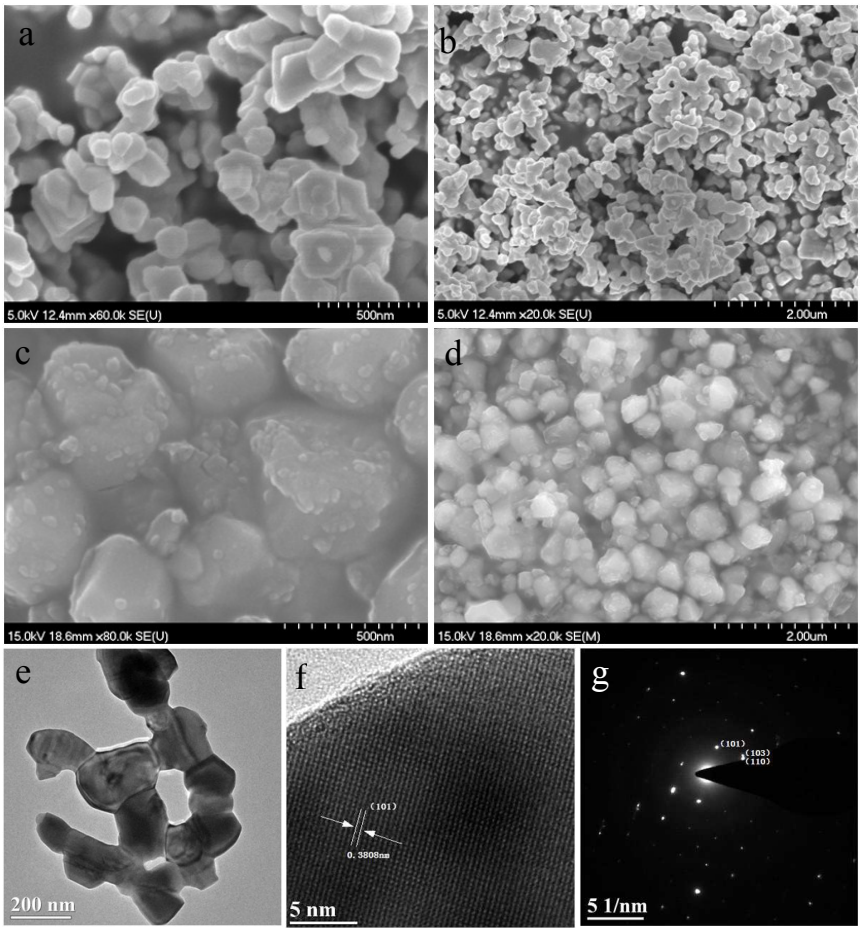

Fig. 1 SEM images of the hydrothermal-LNO nanoparticles (a, b) and Pechini-LNO particles (c, d), TEM, HRTEM images of hydrothermal-LNO nanoparticles (e, f) and corresponding to SAED patterns (g).

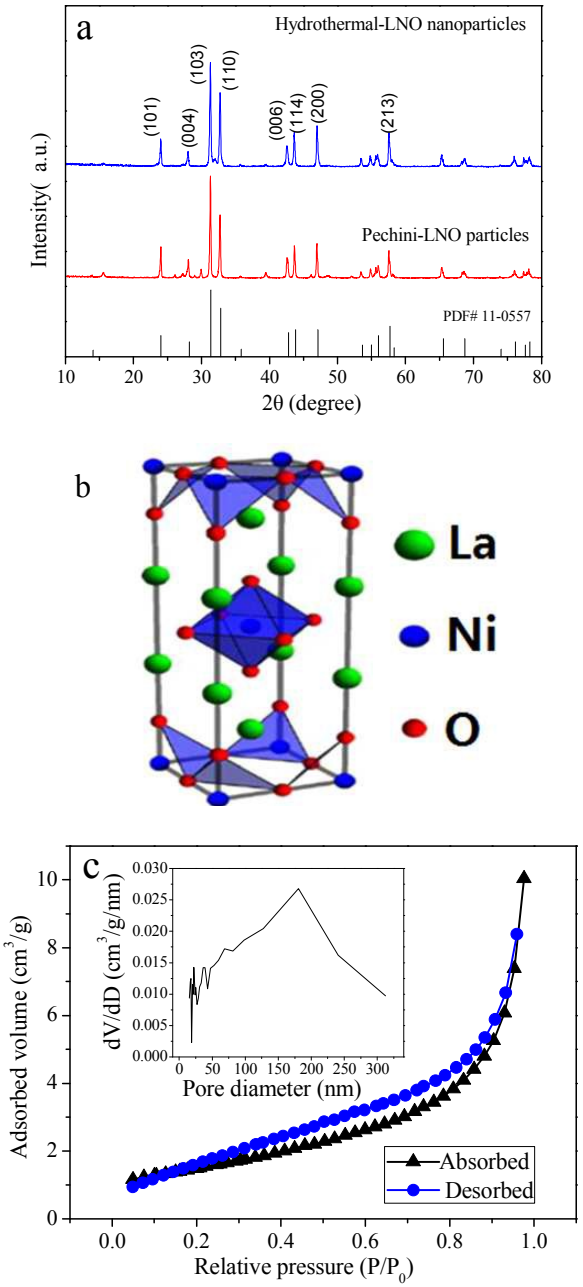

Fig. 2 (a) XRD pattern of the hydrothermal-LNO nanoparticles and Pechini-LNO particles; (b) schematic illustration of the LNO; (c) nitrogen adsorption-desorption isotherms and pore size distribution (inset) of hydrothermal-LNO nanoparticles.

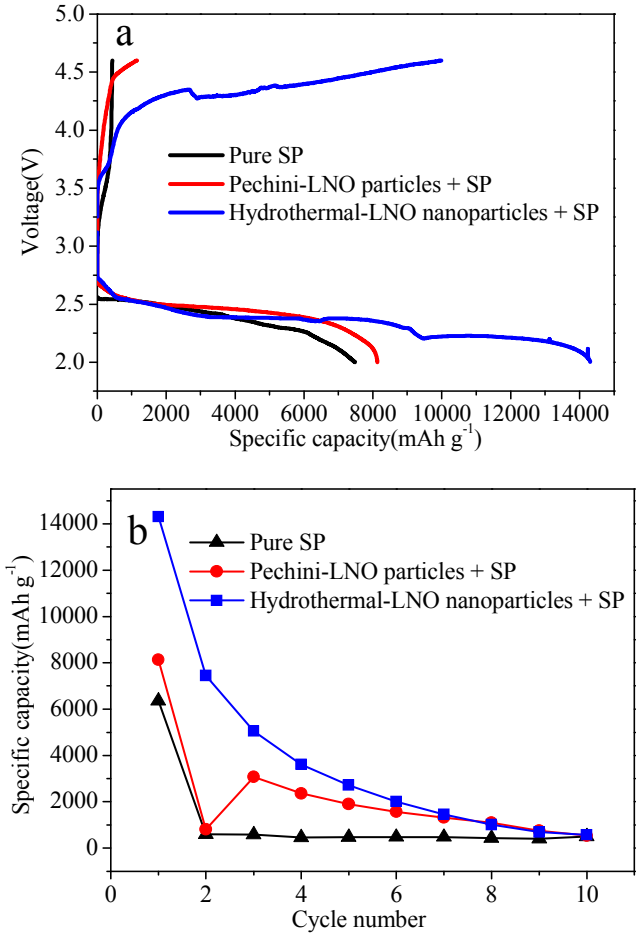

Fig. 3 (a) First discharge-charge curves of Lithium-oxygen batteries with pure SP, Pechini-LNO particles + SP and hydrothermal-LNO nanoparticles + SP electrodes at current density of 0.16 mA cm^{-2}; (b) The cycle ability obtained between 2.0 and 4.6 V at current density of 0.16 mA cm^{-2}.

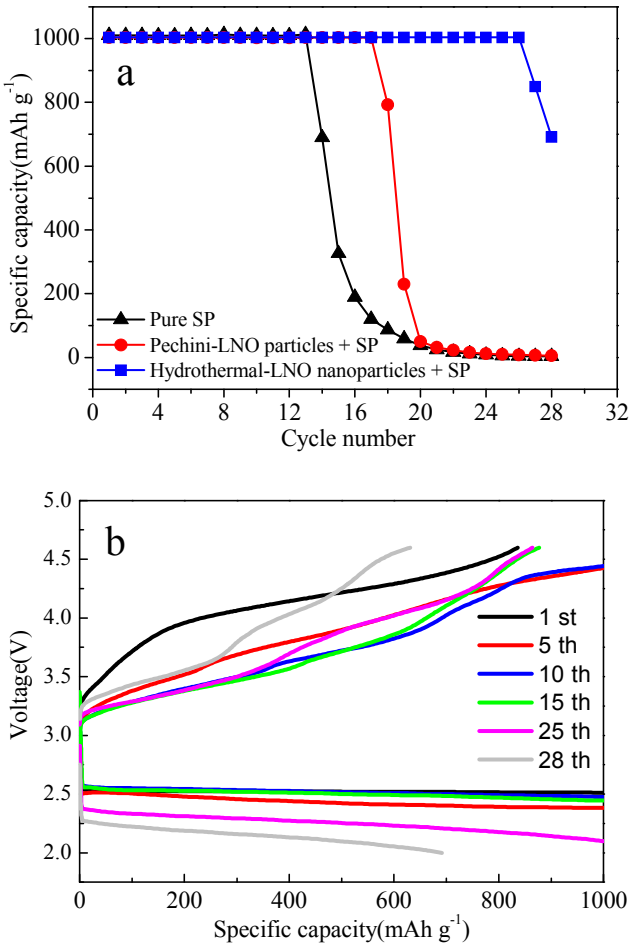

Fig. 4 (a) The cyclic retention of lithium-oxygen batteries with pure SP, Pechini-LNO particles + SP and hydrothermal-LNO nanoparticles + SP electrodes when the capacity were limited to 1000 mAh g^{-1}; (b) The discharge-charge profiles of hydrothermal-LNO particles + SP electrode at current density of 0.16 mA cm^{-2}.

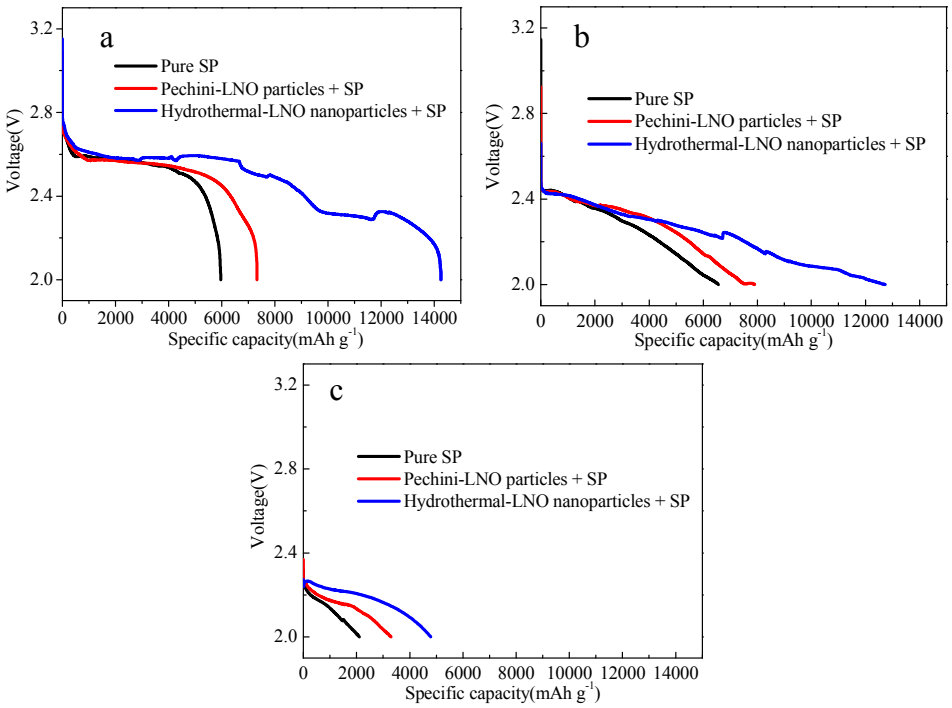

Fig. 5 The initial discharge profiles of lithium-oxygen batteries with pure SP, Pechini-LNO particles + SP and hydrothermal-LNO nanoparticles + SP electrodes at various current densities ((a) 0.08 mA cm^{-2}; (b) 0.32 mA cm^{-2}; and (c) 0.8 mA cm^{-2}).

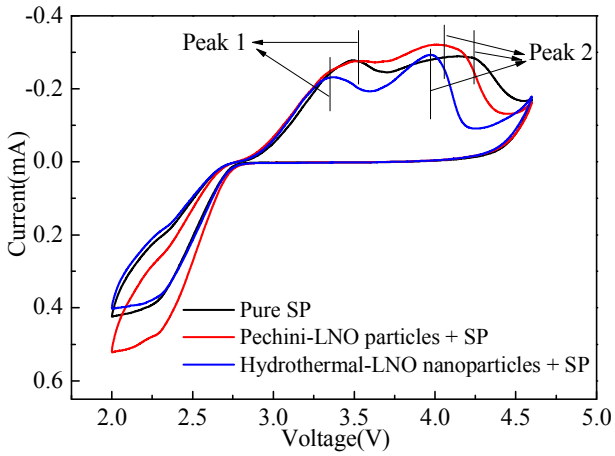

Fig. 6 CV curves of pure SP, Pechini-LNO particles + SP and hydrothermal-LNO nanoparticles + SP electrodes with 1 M LiTFSI/TEGDME at scan rate of 0.1mV s^{-1}.

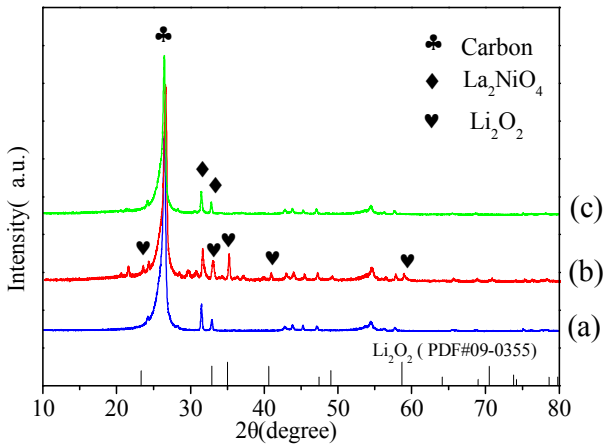

Fig. 7 XRD pattern of the hydrothermal-LNO nanoparticles + SP cathodes at different states ((a) pristine, (b) after 1st discharge and (c) after 1st charge).

Graphical abstract